Bermúdez, JM.; García-Fayos, J.; Reina, TR.; Reed, G.; Persoon, E.; Görtz, D.; Schroeder, M.... (2018). Thermochemical stability of LaxSr1-xCoyFe1-yO3-delta and NiFe2O4-Ce0.8Tb0.2O2-delta; under real conditions for its application in oxygen transport membranes for oxyfuel combustion. Journal of Membrane Science. 562:26-37. https://doi.org/10.1016/j.memsci.2018.05.012

Thermochemical stability of $La_xSr_{1-x}Co_yFe_{1-y}O_{3-\delta}$ and $NiFe_2O_4$-$Ce_{0.8}Tb_{0.2}O_{2-\delta}$ under real conditions for its application in oxygen transport membranes for oxyfuel combustion

Jose M Bermudez[1], Julio Garcia-Fayos[2], Tomas R Reina[1], Graham Reed[1], Emma S Persoon[3], Daniel Görtz[3], Michael Schroeder[3], Marcos Millan[1*], Jose M Serra[2*]

[1] Department of Chemical Engineering, Imperial College London, South Kensington Campus, London, SW7 2AZ, United Kingdom

[2] Instituto de Tecnología Química (Universitat Politècnica de València− Consejo Superior de Investigaciones Científicas), Av. Naranjos s/n, E-46022 Valencia (SPAIN)

[3] Institute of Physical Chemistry, RWTH Aachen Univeristy, Landoltweg 2, 52056 Aachen, Germany

[*] Corresponding Author: jmserra@itq.upv.com; marcos.millan@imperial.ac.uk

Abstract

This work addresses the thermochemical stability of ceramic materials –typically used in oxygen transport membranes– under the harsh gas environments found in oxyfuel combustion processes. Specifically, a dual-phase $NiFe_2O_4$-$Ce_{0.8}Tb_{0.2}O_{2-\delta}$ (NFO-CTO) composite and a single-phase $La_{0.6}Sr_{0.4}Co_{0.2}Fe_{0.8}O_{3-\delta}$ (LSCF) were studied. The effect of the main contaminants present in this kind of processes (CO_2, SO_2 and H_2O) has been tested. NFO-CTO composite remains stable under all the conditions studied whereas LSCF presents a poor stability in the presence of CO_2 and SO_2. Regardless of the treatment, NFO-CTO conserves its crystalline structure, without giving rise to new species due to segregation or incorporation of sulphur and/or carbon. On the contrary, LSCF is prone to degradation in contact with CO_2 and SO_2, segregating Sr in the form of $SrCO_3$ and $SrSO_4$ and Co and Fe in the form of CoO and Fe_3O_4. It is also shown that SO_2 interaction with LSCF is stronger than in the case of CO_2. A concentration of just 2000 ppm of SO_2 in CO_2 is enough to subdue the formation of $SrCO_3$, promoting the segregation of Sr only in the form of $SrSO_4$. With the results presented in this work, it is possible to conclude that the NFO-CTO is a suitable candidate from the thermochemical viewpoint to be used as membrane material in 4-end modules for oxygen generation integrated into oxyfuel combustion processes whereas the use of LSCF should be dismissed.

1. Introduction

Advanced oxyfuel combustion schemes employ pure oxygen mixed with recycled exhaust gases instead of air to carry out the combustion. These technologies will enable efficient CO_2 capture due to the production of almost pure CO_2 in the exhaust gases, since there is no dilution in N_2 as in the case of conventional combustion using air [1, 2]. Other benefits of oxyfuel combustion are the lower NO_x and SO_x emissions and the potential applicability in both new and existing plants through retrofitting [2-4]. These features have attracted high interest in recent years and different technical reports have pointed out that this technology is expected to be ready for commercialisation in a range of 10-20 years [3]. Figure 1 shows a typical block diagram of an oxyfuel combustion process. Nowadays, oxygen separation from air is based on cryogenic distillation and pressure swing technologies. However, these processes give rise to important energy penalties, which fall in the range of 8-12 %. This is a drawback that still remains to be sorted out and that can compromise the viability of the whole process [1, 3]. For this reason, the use of oxygen transport membranes (OTMs) is an appealing alternative technology for air separation due to its lower energy requirements [5, 6].

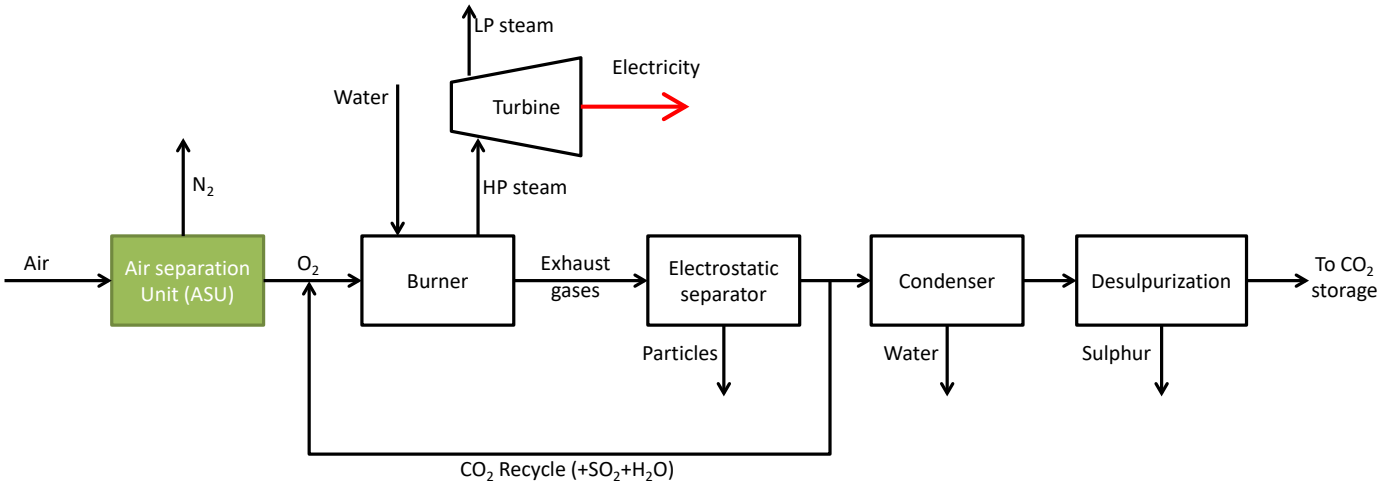

Figure 1. Block diagram of an oxy-combustion process with the air separation unit highlighted in green (HP: High pressure; LP: Low pressure)

Mixed ionic-electronic conductors (MIEC) are a family of materials with huge potential for their application in fields like solid oxide fuel cells or OTMs [7-9]. These materials are able to transport both ions (such as O^{2-} or H^+) and electronic charge carriers (electrons/holes) [10]. As a consequence, their use in oxygen separation by means of oxygen transport membranes is awakening much interest in research [8]. OTMs are gas-tight membranes that can transport oxygen ions when a gradient of oxygen partial pressure (pO_2) is applied through them. When this gradient of partial pressure is applied, O^{2-} ions are transported from the side of higher pO_2 (air feed/retentate side) to the side of the lower pO_2

(sweep/permeate side) owing to the presence of defects in the crystal lattice of MIECs [7, 8]. Simultaneously, electron holes are transported in the opposite direction, to compensate the movement of anions, avoiding the use of an external electrical circuitry [9]. Consequently, these materials are only permeable to oxygen, providing a 100 % of selectivity [7, 8]. The typical MIECs for the application in OTMs are single phase perovskites (ABO_3) or fluorites (AO_2) [8].

Nevertheless, the future application of OTMs depends on their ability to reduce the energy penalty associated with the high temperatures needed for oxygen transport and this strongly depends on the degree of integration of the membrane modules [3, 11]. The separation driving force (pO_2 gradient) is built by increasing the air feed pressure [8]. However, this gives rise to an increase in the energy consumption of the air separation process (thus affecting the global energy penalty). In addition, the membrane is subjected to an important stress due to the pressure difference between both sides of the membrane. This leads to issues related to the mechanical resistance of the materials used, which become more severe at the high operating temperatures of the modules (around 800 ºC). For this reason, an interesting alternative is the application of the so-called 4-end module (Figure 2) [11, 12]. This design is based on the use of the exhaust gases from the oxy-combustion process to sweep the permeate side of the membrane. Indeed, these gases do not contain much oxygen, O_2 concentration in the permeate is assumed to be lower than 1%. Studies about the implementation of the 4-end module concept have found that the drop in the overall plant efficiency can be limited to 5.2 % [3]. However, these gases are composed mainly by CO_2 with small amounts of SO_2 and different contents of moisture. The concentration of SO_2 and moisture depends on the fuel used in the combustion [13, 14]. Table 1 shows CO_2, SO_2 and H_2O concentrations in the exhaust gases from different coal oxy-combustion processes that have been previously reported. These three gases (CO_2, SO_2 and H_2O) can have a critical effect on the thermochemical stability of single phase MIECs [8, 13, 15, 16].

Table 1. Reported CO_2, SO_2 and H_2O composition in exhaust gases from coal oxy-combustion processes.

CO_2 (vol % on a dry basis)	SO_2 (ppm a dry basis)	H_2O (vol %)	Reference
n.a.(1)	< 1000	n.a.(1)	[13]
90-95	1500-1800	n.a.(1)	[17]
n.a.(1)	1000-3000	n.a.(1)	[18]
80-95	600-700	n.a.(1)	[19]
60-90	1000-9000	10-40	[20]
67-72	800-1600	21	[21]
40-85	n.a.(1)	10-60	[22]

(1) n.a.: not available

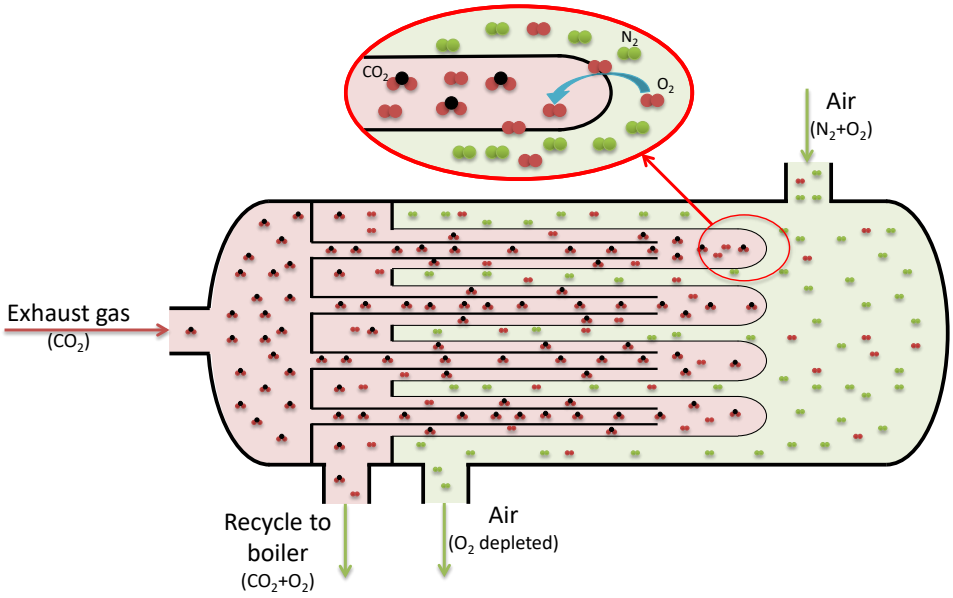

Figure 2. Schematic representation of a 4-end module for application of OTMs in oxy-fuel combustion.

Single-phase perovskites that present good performance in terms of oxygen permeability under clean conditions, like $Ba_xSr_{1-y}Co_yFe_{1-y}O_{3-\delta}$ and $La_{1-x}Sr_xCo_yFe_{1-y}O_3$ (with O_2 fluxes above 2 $ml \cdot min^{-1} \cdot cm^{-2}$ at 850 ºC [23, 24]) are not stable against the presence of both CO_2 and SO_2, and in addition, they suffer a dramatic drop in O_2 to nearly zero in atmospheres with only 10-15% CO_2 and when exposed to SO_2 [25-27] making them unsuitable for oxyfuel applications. These perovskites easily form carbonates and sulphates (mainly Ba and Sr carbonates/sulphates) or undergo phase segregation [13, 16]. This was also observed in several works focused on $La_{0.6}Sr_{0.4}Co_{0.2}Fe_{0.8}O_{3-\delta}$ stability when used as SOFC cathodes exposed to CO_2 and SO_2 [28-30], as well as for similar perovskites consisting of $La_{0.6}Sr_{0.4}CoO_{3-\delta}$ [31, 32]. In addition, the presence of steam in the system affects both the oxygen transport properties and the thermochemical resistance of MIECs [15, 33-35]. According to Wang et al. [34], when moisture content is low, it can have some beneficial effect, facilitating the recombination of the oxygen ions to molecular oxygen on the membrane surface. However, when moisture content is high, H_2O can be adsorbed on the membrane surface, thus blocking the oxygen vacancies. From the thermochemical stability point of view, the presence of steam can promote the formation of new species, such as metal hydroxides, that will modify the transport properties [34, 36]. In addition, when both CO_2 and H_2O are present in the gas stream, there is a synergistic effect that promotes the formation of $SrCO_3$ [15, 35]. On the other hand, single-phase perovskites stable against these gases present poor O_2 permeability [37]. Thus, it is necessary to develop materials that can combine high oxygen permeability and good thermochemical stability in the operating conditions. Dual-phase MIECs appear as a potential alternative able to achieve this objective. In dual-phase membranes, one phase (normally doped ZrO_2 or CeO_2-based fluorite) provides the ionic conductivity while the other phase provides the electronic

conductivity [38]. Initially, ceramic-metal systems, in which noble metals were used as electronic conductors, were proposed. However, this alternative has already been discarded due to the high cost imposed by the use of these expensive metals. Nowadays, combinations of spinel-fluorite and perovskite-fluorite are being studied as potential substitutes of ceramic-metal systems [39-41]. In spite of the encouraging results from these studies, until now there is no membrane that combines both high permeability and thermochemical resistance under real conditions.

An interesting dual-phase MIEC candidate for this application is Ni_2FeO_4-$Ce_{0.8}Tb_{0.2}O_2$ (NFO-CTO) [40, 42]. It has been found that 10 μm-thick membranes built with this composite can achieve high O_2 flux rates of up to 2.5 $ml \cdot min^{-1} \cdot cm^{-2}$ at 850 ºC under clean conditions [43], as well as showing resistance to some extent against CO_2, SO_2 and H_2O [44]. Furthermore, promising O_2 fluxes under CO_2 and SO_2 atmospheres have been obtained with 0.7 mm-thick NFO-CTO membranes [45]. However, its thermochemical resistance against the presence of these gases needs to be tested in environments that simulate real conditions in a 4-end module for OTMs. This work addresses the stability of a NFO-CTO composite in the presence of CO_2, SO_2 and H_2O under close-to-real conditions and compares it with a state of the art single-phase perovskite ($La_{1-x}Sr_xCo_yFe_{1-y}O_3$) in order to determine the potential of NFO-CTO for its application as composite for OTMs.

2. Experimental

2.1. Materials

Two different MIECs were used in this study, a single phase $La_{0.6}Sr_{0.4}Co_{0.2}Fe_{0.8}O_{3-\delta}$ (LSCF, provided by H.C. Starck GmbH for thermochemical stability tests and made at RWTH Aachen for the long term stability tests) and a dual phase $NiFe_2O_4$-$Ce_{0.8}Tb_{0.2}O_{2-\delta}$ (NFO-CTO) prepared by Instituto de Tecnología Química. LSCF was prepared in the form of powder and in the form of disks. The powder was used with the aim of maximizing the contact between the gases and the materials, thus enhancing the reactions that may occur and facilitating the study of the stability of the materials. The compact disks, tested in long-term stability experiments, were used with the objective of simulating the conditions that will take place in real modules of OTMs where dense membranes will be in contact with the gases. Similarly, the NFO-CTO composite was prepared in the form of loose powder and compact disks. In addition, a series of specimens were prepared also in the form of prismatic bars to study potential sintering effects of the treatment in the two phases of the composite.

LSCF was synthesized by a sol-gel Pechini route using nitrate precursors[46]. The powder was ball-milled in ethanol for 4 h, pressed into disc shaped samples and sintered at 1200 °C for 5 h. The dense samples were polished and divided into four 7 x 7 mm pieces. The NFO-CTO composite powder was

prepared by a one-pot Pechini process, which yields powder with both phases being better intermixed than the solid state synthesis method [16]. Transition metal and lanthanide nitrates were dissolved in distilled water solution. $Ce(NO_3)_3 \cdot 6H_2O$ and $Fe(NO_3)_3 \cdot 9H_2O$ were provided by Sigma Aldrich. $Tb(NO_3)_3 \cdot 6H_2O$ and $Ni(NO_3)_3 \cdot 6H_2O$ were provided by ABCR GmbH. After all salts were dissolved, citric acid (Sigma Aldrich) was added as chelating agent to prevent partial segregation of metals. Ethylene glycol was then added to polymerize with the chelating agent, producing an organometallic polymer (molar ratio metal:chelating agent:gelating agent 1:2:4). Complexation and gelation were followed by dehydration in air at low temperature (up to 270 °C). Thermal decomposition of the precursors was carried out at 750 °C in air, obtaining the composite powders with the correct structural phases (fluorite for the CTO and spinel for the NFO). Finally, the composite powder was sintered at 1200 ºC in air during 4 hours, thus reproducing sintering conditions of NFO-CTO when deposited as catalytic layer on a membrane. Dense bars were obtained by uniaxially pressing the composite powder in bars of 40 mm of length and 5 mm^2 of base at 125 MPa and subsequently calcining them at 1400 °C for 10 h (2 $ºC \cdot min^{-1}$ heating rate, 5 $ºC \cdot min^{-1}$cooling rate). A schematic figure with the preparation method of the powder, disks and bars of NFO-CTO was included in the Supplementary Info (Figure S1). The dense disks were prepared following the same procedure as for LSCF. The disks and bars presented a density of 98%.

2.2. Thermochemical stability testing

The thermochemical testing of the powder samples and the dense bars (in the case of NFO-CTO) was performed in an up-flow vertical testing unit made of quartz (Figure 3). The testing unit consisted of a quartz liner containing a porous plate to hold the sample and distribute the gas evenly during the treatment. A thermocouple was placed in the middle of the material bed to monitor the temperature during the treatment.

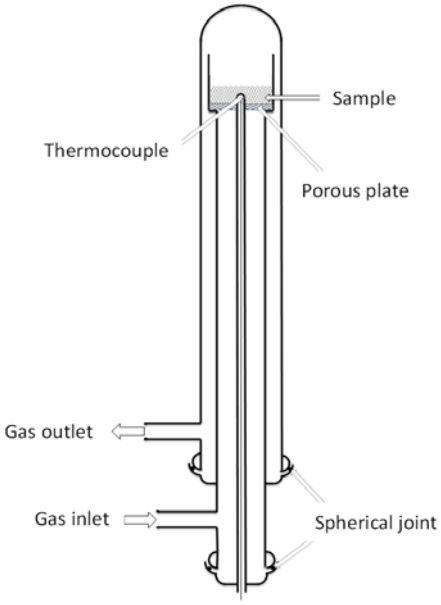

Figure 3. Scheme of the quartz liner of the testing unit used for the thermochemical testing of the MIEC powders.

Approximately 1 g of fresh powdered sample (along with the pellets in the case of NFO-CTO) was placed in the quartz testing unit, which was introduced in a vertical furnace chamber heated by SiC rods. Once the unit was introduced in the chamber, it was heated up to the reaction temperature under air atmosphere. The experiments were performed at atmospheric pressure and at 850 ºC and 900 ºC. Once the temperature was reached, the gaseous mixture started to be fed. Different gaseous mixtures were used to test the effect of the different components upon the material. Table 2 summarizes the composition of the gaseous streams used in the stability tests.

Table 2. Conditions of the thermochemical stability tests performed with the powders and the pellets.

Test	Temperature (ºC)	Feed dry gases		Added
		CO2 (% vol)	SO_2 (ppm)	H_2O (% vol.)
Blank 850	850	100	0	0
Blank 900	850	100	0	0
500SO_2 850	900	99.95	500	0
500SO_2 900	900	99.95	500	0
100SO_2 10H_2O 850	850	99.99	100	10
500SO_2 10H_2O 850	850	99.95	500	10
2000SO_2 10H_2O 850	850	99.8	2000	10
500SO_2 30H_2O 850	850	99.95	500	30

Initially, a series of experiments at 850 ºC and 900 ºC with CO_2 and mixtures of 500 ppm of SO_2 in CO_2 were performed with the aim of addressing the effect of these gases on the materials at different

temperatures. Then, moisture was added to study its influence on the process. Finally, the concentration of SO_2 and the moisture contents were varied. The levels of SO_2 and H_2O were chosen according to the different conditioning options for exhaust gases that might be available in oxyfuel combustion plants. These gases can be conditioned prior entering the OTM module with the aim of partially removing the SO_2 and/or their moisture content. Although this goes against the efficiency of the overall process (gas conditioning involves energy consumption), it can help to use MIECs that could be resistant against SO_2 and H_2O up to a threshold in concentration but that present low resistance when this threshold is surpassed. For this reason, it is necessary to study the effect of the concentration of SO_2 and the moisture content, with the aim of determining the harshest conditions at which the MIECs can operate without degradation. In this work, three levels of SO_2 concentration have been defined:

- Level 1: 100 ppm. To achieve such a low SO_2 concentration it is necessary to carry out desulphurization at low temperatures, which will result in important losses of energy efficiency because the exhaust gases have to be re-heated prior to their introduction in the OTM module.
- Level 2: 500 ppm. This level of desulphurization can be achieved at high temperatures, thus reducing the energy penalty associated to Level 1.
- Level 3: 2000 ppm. No desulphurization treatment is needed, thus maximizing energy efficiency.

Similarly to the procedure with SO_2, three levels of moisture have been defined:

- Level 1: 0 % vol. All the moisture is removed from the exhaust gases. This will require a condensation unit that will consume important amounts of energy and a subsequent re-heating unit. Consequently, this will lead to remarkable energy penalties.
- Level 2: 10 % vol. Partial removal of the moisture is needed. This will give rise to energy penalties, although considerably lower than those from Level 1.
- Level 3: 30 % vol. This level will not need any condensation of the moisture, thus avoiding associated energy penalties in the whole process.

Combining the three levels defined for SO_2 concentration and moisture content, the experimental design shown in Figure 4 was followed to study the effect of these variables. These experiments were performed at 850 ºC because it was found that the damaging effect of the gases over the LSCF is higher at 850 ºC than at 900 ºC since carbonates and sulphates of the metallic components are less stable at the higher temperature.

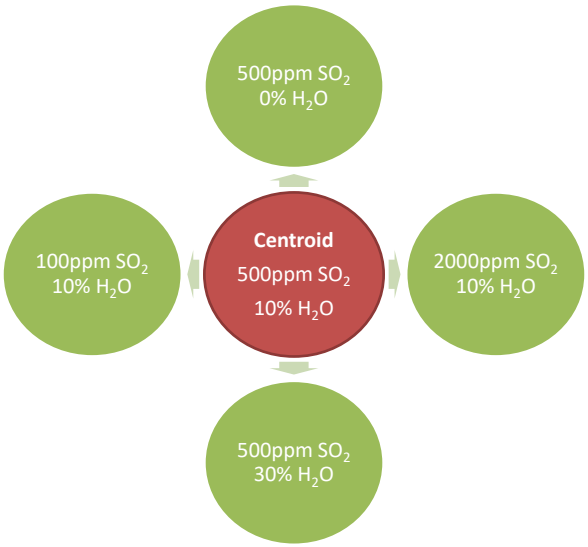

Figure 4. Experimental design for the study of the effect of SO_2 concentration and moisture content on the LSCF and NFO-CTO.

The mixtures of CO_2 and SO_2 were prepared by mixing the gas content of two different gas cylinders containing pure CO_2 and a mixture of 2000 ppm of SO_2 in CO_2. Then, steam was added using an evaporator, composed by a syringe pump and a heated pipe connected to the testing unit. The total flow rate used was 0.25 $NL \cdot min^{-1}$. The outlet gases passed through a gas cooling system with a volume of 0.5 L, where steam was condensed and removed. The cooling system was filled with a basic solution of $Ca(OH)_2$ to neutralize the acidic nature of the water recovered, which contained acid species due to the presence of CO_2 and SO_2 in the system. The dry exhaust gases passed through a series of SO_2 traps to remove this toxic gas prior their release into the ventilation system. The experiments lasted for a total of 8 hours, and then the unit was taken out of the hot chamber and cooled down as quickly as possible under the reaction atmosphere. Once the material reached room temperature, it was recovered for characterization.

For the long-term stability testing of the sintered disks of LSCF and NFO-CTO, a slightly different set-up was employed. Samples were placed on a gold plated sample holder seated on top of an aluminum oxide support tube through which the test gas flowed. Gold plating was applied to prevent chemical reaction between the sample and the aluminum oxide (Figure 5). Test runs were carried out for 200 h at 850 °C and a constant flow of a N_2/SO_2 gas mixture. The flow rate was 50 $NmL \cdot min^{-1}$ and the SO_2 concentration was varied between 2 and 50 ppm.

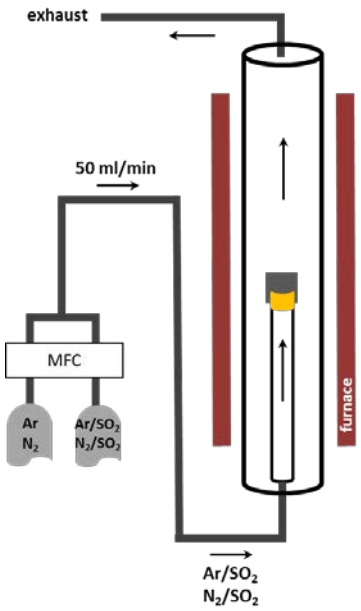

Figure 5. Scheme of the long-term stability test setup for the sintered samples.

2.3. Material characterization

X-ray diffraction (XRD) patterns of the powder samples were obtained using a PANalytical diffractometer equipped with a Ni-filtered Cu Kα radiation. The XRD patterns were processed using the software X'Pert Highscore Plus to identify the species present in the samples. The characterization of the sintered samples was performed with a STOE Theta–Theta XRD reflection diffractometer with Cu-K_α-radiation.

X-ray fluorescence (XRF) was performed to determine the chemical composition of the fresh and spent powders, especially the sulphur content. Measurements were performed using a MiniPal 4 EDXRF spectrometer (PANalytical), equipped with a 30 kV rhodium anode tube. In addition, elemental analysis was used to detect the presence of carbon or sulphur that could have been incorporated during the treatment. These analyses were performed using an EuroVector EuroEA Elemental Analyzer (CHNS), with the combustion chamber operating at 1293.15 K. Flash combustion gases were separated by gas chromatography column and peaks were detected in a thermal conductivity detector (TCD). The TCD signal for each element is translated to weight percentage content.

A Perkin Elmer FTIR 100 spectrometer was used for performing the attenuated total reflection Fourier transform infrared spectroscopy in the powders (ATR-FTIR). Background subtracted spectra of the raw and the treated samples were collected at room temperature by co-adding 32 scans at 4 cm^{-1} resolution in transmittance mode. Data were baseline corrected using Spectrum 10™ software.

Raman spectra of the powdered samples were obtained using a Renishaw inVia Raman spectrometer equipped with a Leica DMLM microscope and a 785-nm Nd ion laser as an excitation source. A x50 objective of 8-mm optical length was used to focus the depolarized laser beam on a spot of about 3 μm in diameter. The Raman scattering was collected with a charged coupled device (CCD) array detector.

Scanning electron microscopy with energy-dispersive X-ray spectroscopy (SEM-EDS) studies of the powders and pellets was done in a JEOL JSM6400 operated at 20 KV. The microscope was equipped with an energy dispersive X-ray spectroscopy (EDS) system. The LSCF disks were characterized in a SEM (LEO/Zeiss, 1450VP, Jena, Germany) with an EDS system (Oxford INCA).

3. Results and discussion

3.1. Thermochemical stability of LSCF

3.1.1. Studies with the powder samples

Figure 6 shows the XRD patterns of the fresh and spent samples of LSCF, treated at 850 and 900 ºC under CO_2 and a binary mixture of 500 ppm of SO_2 in CO_2 and treated with a ternary mixture of 500 ppm of SO_2 in CO_2 with 10 % vol. of moisture at 850 ºC. When LSCF was treated under CO_2 atmosphere, the material was modified. LSCF was still the main component, although the presence of $SrCO_3$ and Fe and Co oxides was clearly identified in the sample. These findings were in agreement with results previously reported by other authors, who also found that Sr and Co strongly segregated from the perovskite structure due to the presence of CO_2 [33, 47]. Sr reacts easily with CO_2 to form $SrCO_3$ due to its low chemical potential according to the Ellingham diagram (Figure S2 in the Supplementary Information). In the case of Co and Fe, they were segregated from the perovskite in the presence of CO_2 to preserve the overall perovskite structure, compensating for the shortage of A-site metal elements [33, 48]. This segregation resulted in the appearance of LSCF perovskites with different compositions than the original (with less Sr, Fe and/or Co) although their concrete composition has not been determined in this work. When SO_2 was incorporated to the gaseous mixture, the LSCF showed again low stability. $SrSO_4$ appeared as new species in addition to the $SrCO_3$ formed as a consequence of the presence of CO_2 and Fe and Co oxides. Formation of $SrSO_4$ in LSCF perovskites due to exposure to SO_2 atmosphere has been previously observed [13, 49]. Both carbonates and sulphates signals were less intense when the experiments were carried out at 900 ºC, especially in the case of carbonates. This suggested that, at 900 ºC, CO_2 and SO_2 presented lower ability to react with LSCF components to give rise to new phases, due to the lower stability of these phases at this temperature. That means that an increase in the process temperature can help in protecting the LSCF from being damaged by the gaseous atmosphere. However, research efforts are being focused on the opposite direction: decreasing the process temperature, with the aim of decreasing the energy penalties linked to the air separation unit and the requirements for housing and sealing materials.

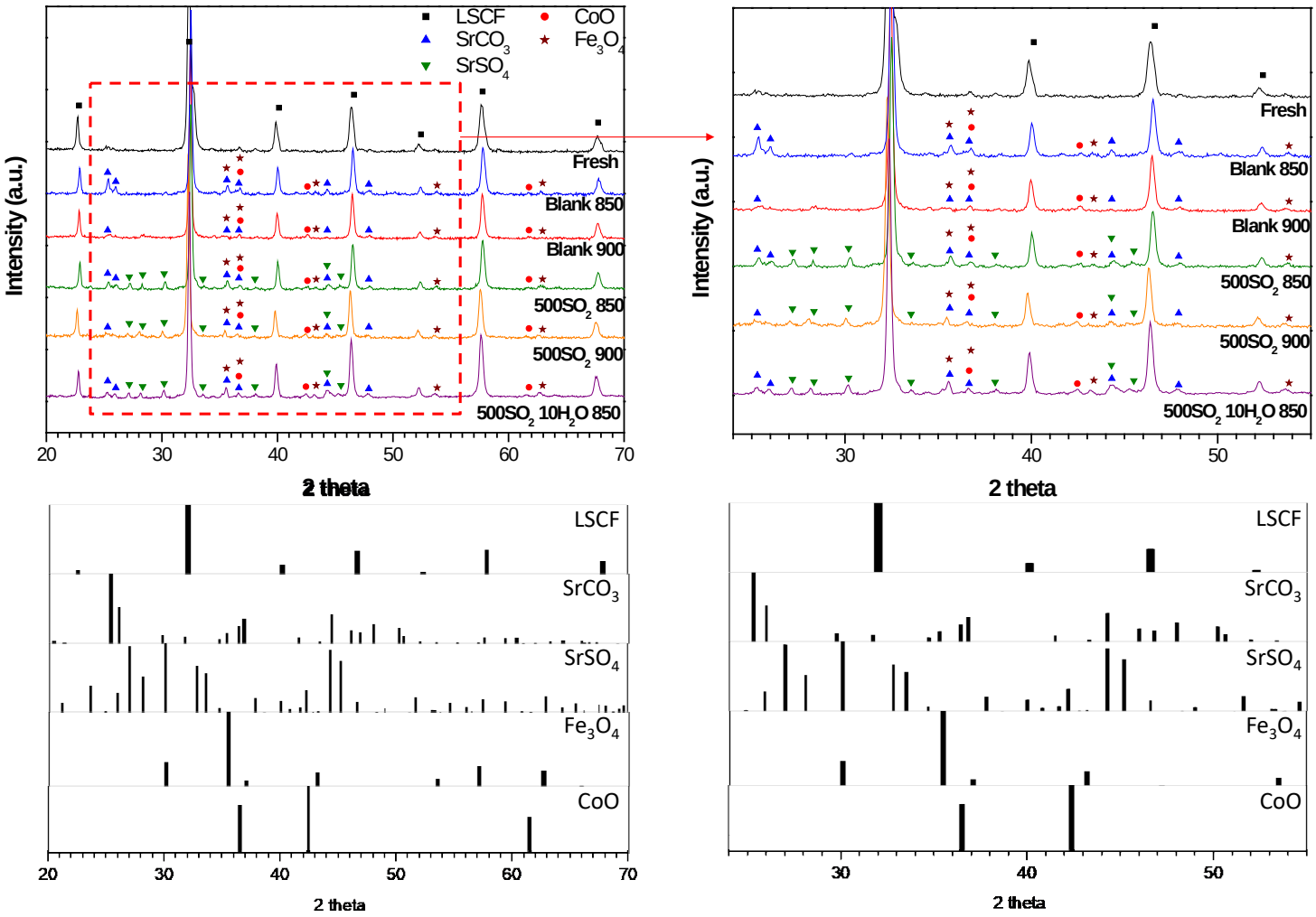

Figure 6. XRD patterns of the LSCF powder samples fresh and treated with CO_2, CO_2/SO_2 and $CO_2/SO_2/H_2O$ mixtures at 850 and 900 ºC and atmospheric pressure. The inset shows a detail of the patterns from 2θ = 24 to 2θ = 55º, where most of the main signals of the new phases are present.

As stated before, steam can affect both the oxygen transport properties and the thermochemical resistance of these materials [15, 33-35]. With the aim of studying the effect of H_2O on the stability of LSCF, a 10 % vol. of steam was added to the experiment carried out with the mixture of 500 ppm of SO_2 in CO_2 at 850 ºC. As shown in Figure 6, there were no new species formed when H_2O was added. The intensity of the peaks belonging to $SrSO_4$ species seemed to increase slightly. However, this is not enough to point to some kind of synergetic effect due to the presence of H_2O, similar to that previously reported between CO_2 and H_2O [15, 35], and this effect would be negligible compared with the damaging effect of the SO_2 alone over the LSCF.

XRD reveals the presence of species only if they form crystalline domains of enough size to be detected by this technique. For this reason, the materials were characterized using ATR-FTIR and Raman

spectroscopy, which are also sensitive to non-crystalline species and more sensitive to small domains. Figure 7 shows the ATR-FTIR and Raman spectra of the fresh and spent samples of LSCF. The results from the ATR-FTIR confirmed the findings from XRD about the poor resistance of LSCF against CO_2 and SO_2. All the spent samples presented bands at 1452 and 1430 cm^{-1} that were not observed in the fresh sample. Bands between 1400 and 1600 cm^{-1} can be assigned to C=O bond stretching in carbonate-like species. In addition, the spent samples also showed a sharp band at 858 cm^{-1}. Bands between 850 and 900 cm^{-1} are characteristic of the out of plane/in-plane bending of CO_3^{2-} [10, 50, 51]. More concretely, Hu *et al.* [52] and Turianicová *et al.* [10] found that $SrCO_3$ gave rise to bands at 855/1430 and 858/1470 cm^{-1} respectively, which matched very well with the bands found in this work at 858, 1430 and 1452 cm^{-1}. The addition of SO_2 gave rise to the appearance of several bands at 993, 1082, 1125 and 1198 cm^{-1}. SO_4^{2-} ions present different absorption signals (symmetric and asymmetric stretching and bending) in the range of 950-1250 cm^{-1}, especially strong in the range of 1080-1125 cm^{-1} [10, 50, 53]. Turianicová *et al.* [10] reported similar bands (993, 1120-1124 and 1198-1205 cm^{-1}) to those shown in this work. The observation of the Raman spectra of the LSCF treated samples allowed identifying a new peak at around 1000 cm^{-1}, which corresponded to the formation of sulphates, confirming again the findings from XRD and ATR-FTIR [42, 54].

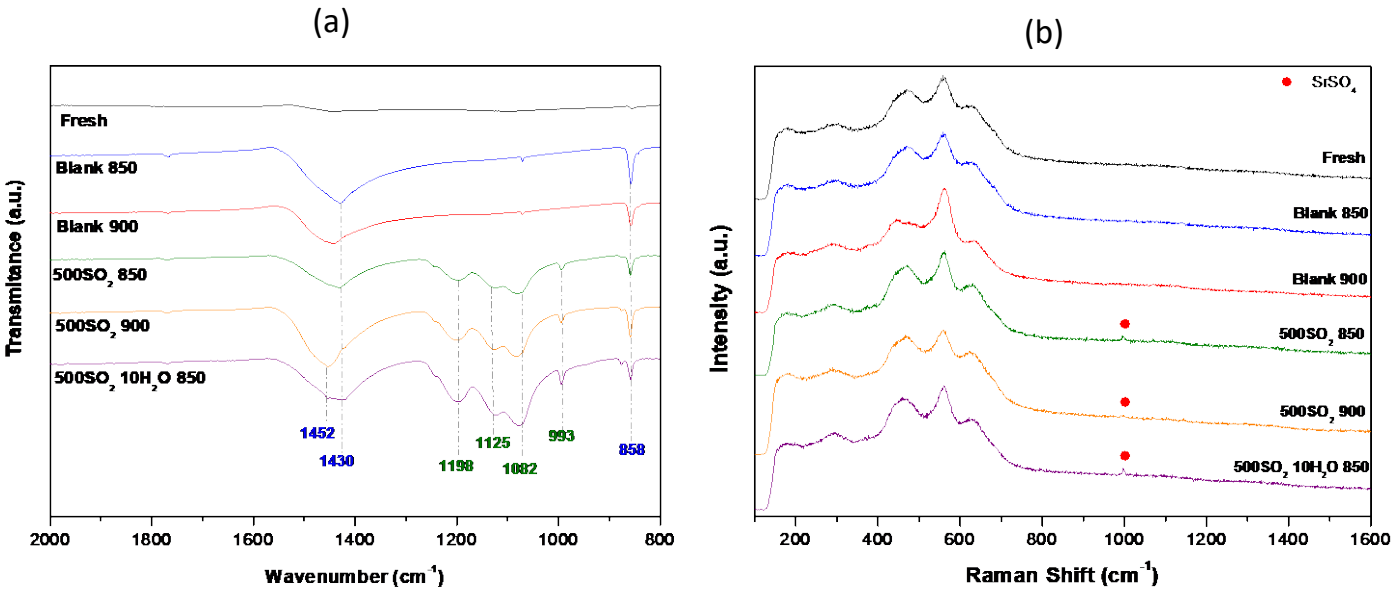

Figure 7. (a) ATR-FTIR (numbers in blue correspond to carbonate signals and numbers in green to sulphate signals); and (b) Raman spectra of the LSCF (powder samples) fresh and treated with CO_2, CO_2/SO_2 and $CO_2/SO_2/H_2O$ mixtures at 850 and 900 ºC and atmospheric pressure.

Figure 8 shows the XRD patterns of the LSCF samples treated with different concentrations of SO_2 and H_2O at 850 ºC. At low SO_2 concentration (100 ppm), the intensity of the $SrSO_4$ signals became very weak whereas the intensity of the $SrCO_3$ signals became much stronger, similar to that from the

experiment with pure CO_2 (see Figure 6). Since the mere observation of the XRD signals is not enough to draw conclusions on the amount of the different phases present in each sample, a Rietveld refinement was used for semi-quantitatively determine the amount of each of these phases in the treated samples. The data corresponding to this refinement are provided in the Supplementary Information (Figure S3, Table S1). As SO_2 concentration rose, the amount of $SrSO_4$ in the treated samples increased while the amount of $SrCO_3$ decreased. The signals of $SrCO_3$ practically disappeared when 2000 ppm of SO_2 were used, decreasing to less than 3% wt. whereas it reached 12% wt. in the experiment performed with 100 ppm of SO_2. The intensities of the peaks belonging to Fe_3O_4 and CoO were almost constant regardless of the concentration of SO_2 used in the treatment. Consequently, the weight percentage of these phases was almost constant in the range of 7-8% wt. for Fe_3O_4 and 1-2% wt. for CoO. These results suggested that the formation of $SrCO_3$ competed with the formation of $SrSO_4$, the latter being much stronger. A concentration of just a 0.2 % vol. (2000 ppm) of SO_2 was enough to practically neutralize the effect of a concentration of 99.8 % vol of CO_2. This way, $SrSO_4$ was almost the only species formed when Sr was segregated from the perovskite. However, the segregation of Fe and Co and the consequent formation of Fe_3O_4 and CoO seem to be constant, regardless of the conditions studied. This could be expected since Fe and Co were segregated to preserve the perovskite structure after the segregation of Sr, irrespective to type of species formed ($SrCO_3$ or $SrSO_4$).

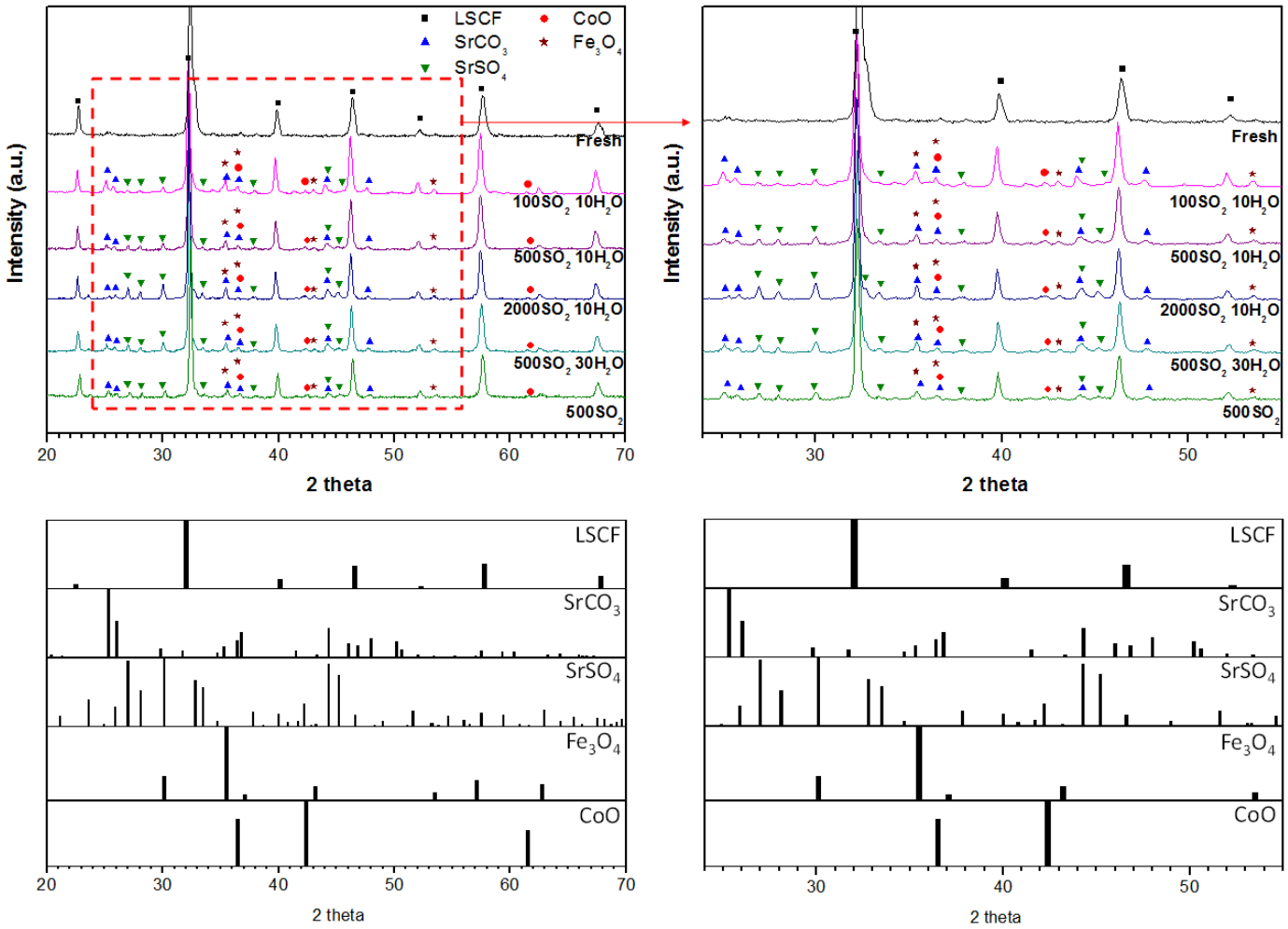

Figure 8. XRD patterns of the LSCF powder samples fresh and treated under different concentrations of SO_2 and H_2O at 850 ºC and atmospheric pressure. The inset shows a detail of the patterns from 2θ = 24 to 2θ = 55º, where most of the main signals of the new phases are present.

The competitive mechanism that was inferred from the XRD analysis was also supported by the FTIR results. As shown in Figure 9a, when the concentration of SO_2 increased the intensity of the peaks corresponding to SO_4^{2-} species grew. On the contrary, the spectrum of the sample treated at 2000 ppm was practically flat in the range of 1300-1600 cm^{-1}, where the signals corresponding to the CO_3^{2-} species should have appeared. This confirmed the idea that a concentration of just 2000 ppm of SO_2 was enough to practically avoid the formation of $SrCO_3$ and the segregation of Sr from the perovskite proceeded to form only $SrSO_4$. Raman spectra (Figure 9b) also confirmed that the increase in SO_2 concentration favoured the formation of SO_4^{2-}, since the intensity of the signal around 1000 cm^{-1} corresponding to SO_4^{2-} increased and a second weak signal around 200 cm^{-1} appeared for the first time when a concentration of 2000 ppm of SO_2 was used [42, 54].

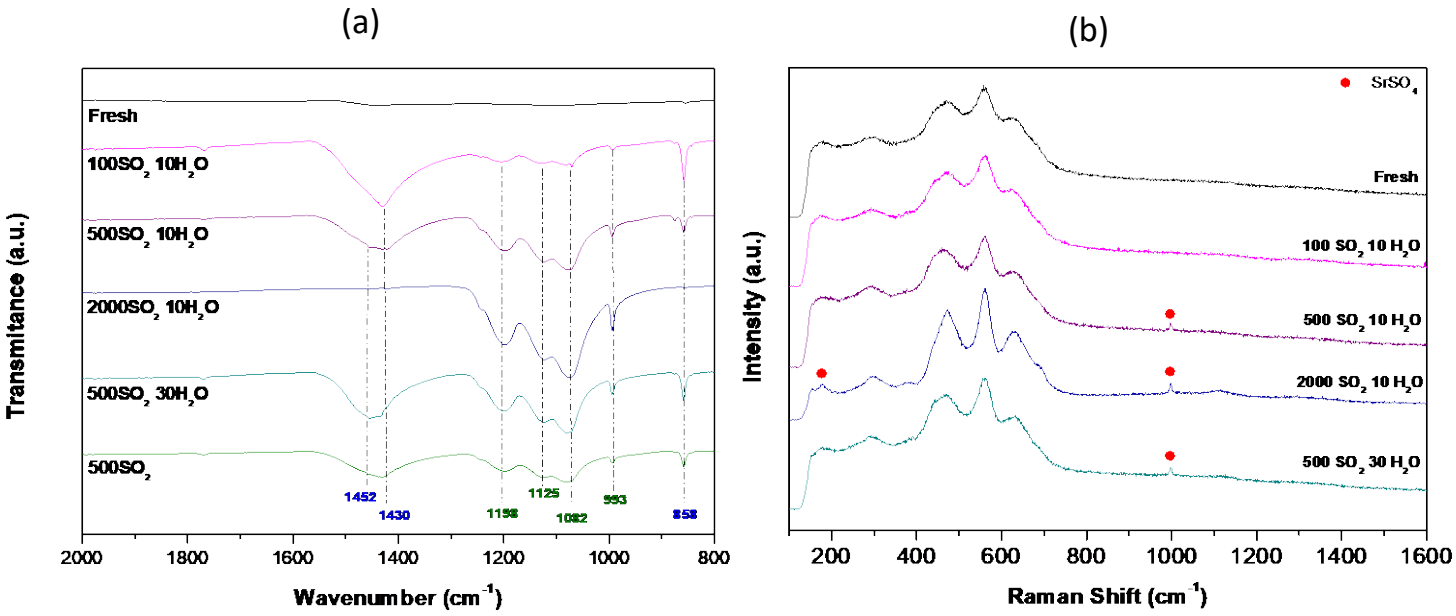

Figure 9. (a) ATR-FTIR; and (b) Raman spectra of the LSCF (powder samples) fresh and treated under different concentrations of SO_2 and H_2O at 850 ºC and atmospheric pressure.

With the aim of semi-quantitatively determine the incorporation of C and/or S to the samples, as the identified species or as any other species not identifiable by means of XRD or vibrational spectroscopy, C and S contents were determined by means of elemental analysis and XRF. Results from the elemental analysis are shown in Table 3 (XRF, not shown, presented the same trends). Carbon was found in all the treated samples whereas sulphur was observed in all the experiments in which SO_2 was added to the gaseous stream.

Table 3. Elemental analysis of carbon and sulphur content in the fresh and treated samples of LSCF and NFO-CTO. Note: experimental error ±0.2%. (1) n.d.: not detected (below the limit of detection)

		Elemental Analysis	
		Sulphur (wt. %)	*Carbon (wt. %)*
LSCF	Blank 850	-	1.4
	500SO_2 850	2.3	0.7
	100SO_2 10H_2O 850	0.7	1.2
	500SO_2 10H_2O 850	2.2	0.7
	2000SO_2 10H_2O 850	4.5	0.1
	500SO_2 30H_2O 850	2.1	0.7
NFO-CTO	Blank 850	-	n.d.(1)
	500SO_2 850	n.d. (1)	n.d. (1)
	100SO_2 10H_2O 850	n.d. (1)	n.d. (1)
	500SO_2 10H_2O 850	n.d. (1)	n.d. (1)
	2000SO_2 10H_2O 850	n.d. (1)	n.d. (1)
	500SO_2 30H_2O 850	n.d. (1)	n.d. (1)

3.1.2. Studies with dense sintered samples

Sintered samples were tested for long-term stability (up to 1000 h). The diffraction patterns of the fresh LSCF sintered sample and of the samples subjected to 2, 10, 25 and 50 ppm of SO_2 are shown in Figure 10. The perovskite diffraction peaks of all the samples subjected to SO_2/N_2 were shifted to smaller angles. This indicated that a lattice expansion occurred. The diffraction patterns of the samples subjected to 2, 10, 25 and 50 ppm SO_2 showed additional peaks corresponding to $SrSO_4$. The intensities of these peaks did not exactly correspond to the intensities of the diffraction pattern due to a preferred orientation of the $SrSO_4$ crystals on the surface, which was most noticeable in the sample subjected to 50 ppm SO_2.

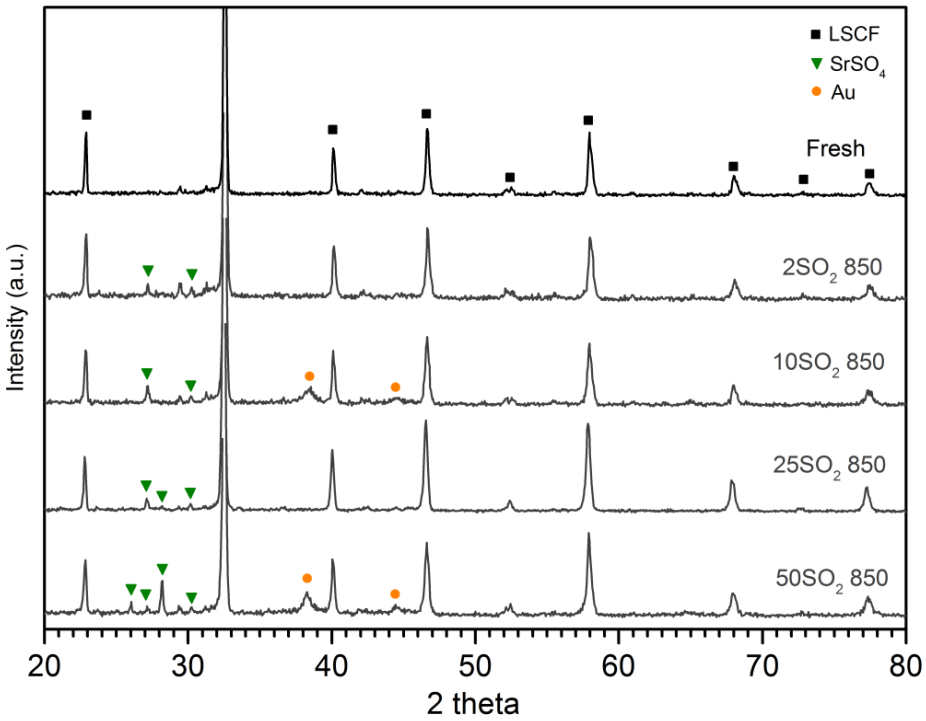

Figure 10. XRD patterns of the LSCF sintered disks fresh and treated with 2, 10, 25 and 50 ppm of SO_2 at 850 °C and atmospheric pressure.

Crystals were formed on the surface of all LSCF treated samples. The higher the concentration of SO_2 during the stability test, the larger the crystals grow on the surface. Even on the surface of the sample subjected to 2 ppm SO_2, sulfur-containing crystals were detected. A SEM image and EDS mapping of a wedge-shaped crystal on the surface of the sample subjected to 50 ppm SO_2 are shown in Figure 11. The crystal contained a high amount of sulfur as shown in the mapping (Figure 11b). Part of the surface area around the long wedge-shaped crystal presented a lighter colour (Figure 11a). This lighter area (marked by red arrows in the image) was ~~completely~~ depleted of strontium (Figure 11c) but was rich in

lanthanum (Figure 11d). Thus it can be concluded that strontium diffused from the bulk LSCF material to the surface forming crystals that consisted of strontium, sulfur and oxygen.

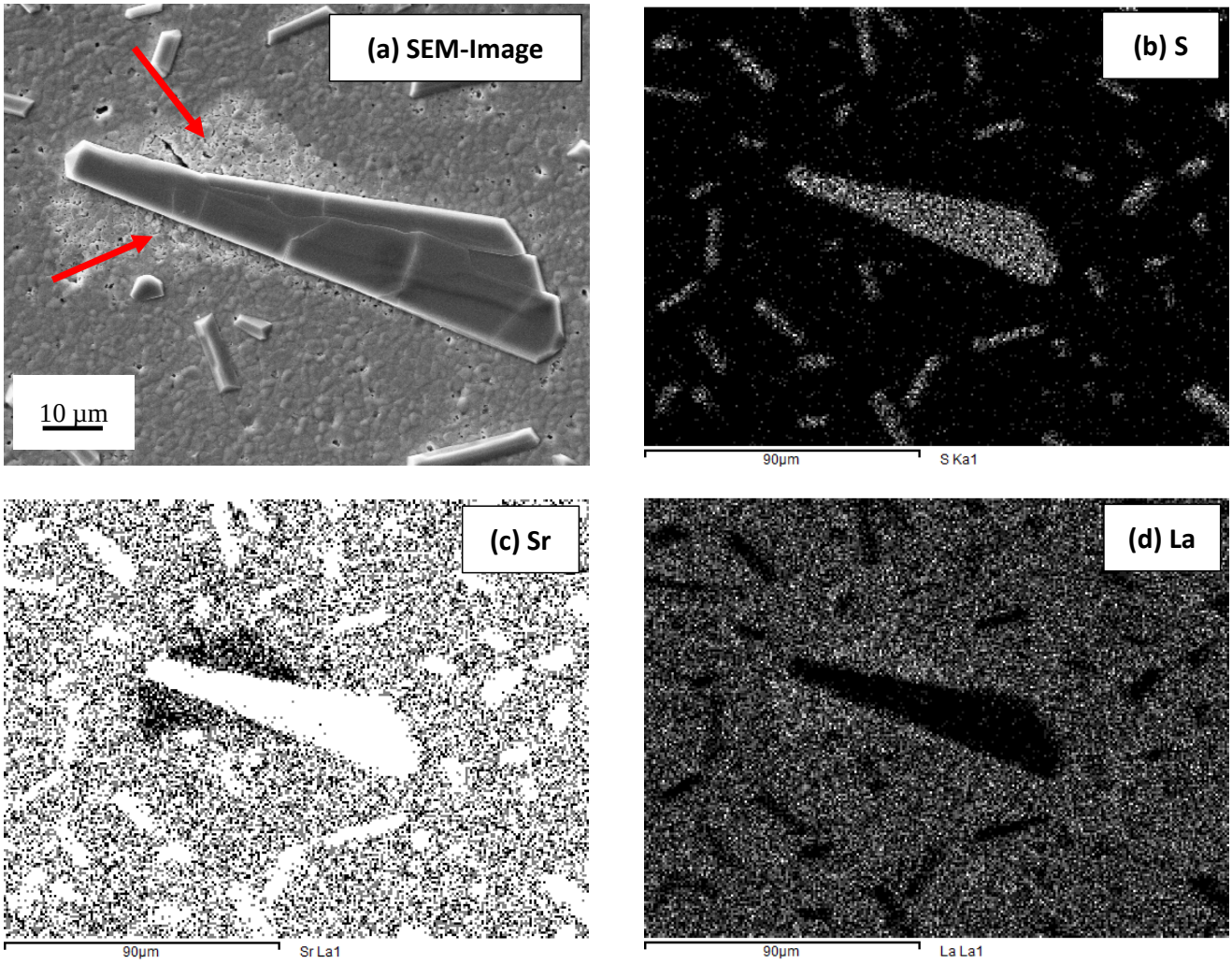

Figure 11. (a) SEM image of a wedge-shaped crystal in the LSCF surface formed after the treatment with 50 ppm of SO_2 (the red arrows mark the Sr-depleted light area); (b) sulphur, (c) strontium and (d) lanthanum EDS mapping of the LSCF surface after stability test in 50 ppm SO_2/N_2.

3.2. Thermochemical stability of NFO-CTO

3.2.1. Studies with the powder samples

Figure 12a shows the XRD spectra of the NFO-CTO samples fresh and treated at 850 and 900 ºC with CO_2, a mixture of 500 ppm of SO_2 in CO_2 and a mixture of 500 ppm of SO_2 in CO_2 adding a 10 % vol. of moisture at 850 ºC. The NFO-CTO showed very high stability since no new species were identified. The treated dual-phase composite conserved exactly the same composition and structure as the fresh sample under all the different conditions studied. In this case, the high stability of the NFO-CTO against

CO_2 can be explained by the high resistance shown by each of its oxide components alone. In the case of the ionic conductor, it has been reported that the chemical stability of fluorites, and more concretely doped ceria, is very high in the presence of CO_2 (especially higher than in the case of perovskites) [39, 55, 56]. Regarding the electronic conductor, the spinel $NiFe_2O_4$, it cannot give rise to Ni or Fe carbonates at the temperatures studied in this work. According to the Ellingham diagram, Ni and Fe carbonates are not stable at these temperatures (Figure S2 in the Supplementary Information) [57]. Some studies in catalysis for hydrocarbon processing have reported that the spinel structure can be broken to give rise to metallic Ni and Fe oxides, but this behaviour would probably be due to the interaction of the spinel with hydrocarbons, since according to the results reported here, no segregation of Ni or formation of Fe oxides were observed [58]. When SO_2 was added to the gaseous stream, the result was exactly the same, since no new peaks could be observed in the X-ray patterns. Although SO_2 can be adsorbed on ceria at low temperature forming bulk sulphate species, ceria is very stable against SO_2 at the temperatures used in this study [59-61]. Moreover, there are references in catalysis where CeO_2 is used to improve catalyst resistance against sulphur poisoning [62-65]. In the case of $NiFe_2O_4$ spinel, the literature available is again scarce. Ni is the metal with higher potential to be sulphidized in the presence of sulphur gases, as has been reported in works using the NFO spinel in sulphur laden reducing atmospheres [58, 66]. However, according to previous studies, Ni sulphates are not stable at temperatures higher than 800 ºC, which may explain the absence of sulphur species in the spent samples [54, 66]. Finally, when steam was added, the material conserved again its structure and no changes or new species could be identified. Therefore, the possible synergetic effect between H_2O and SO_2 inferred in the case of the LSCF was not enough to promote the formation of sulphates in the NFO-CTO.

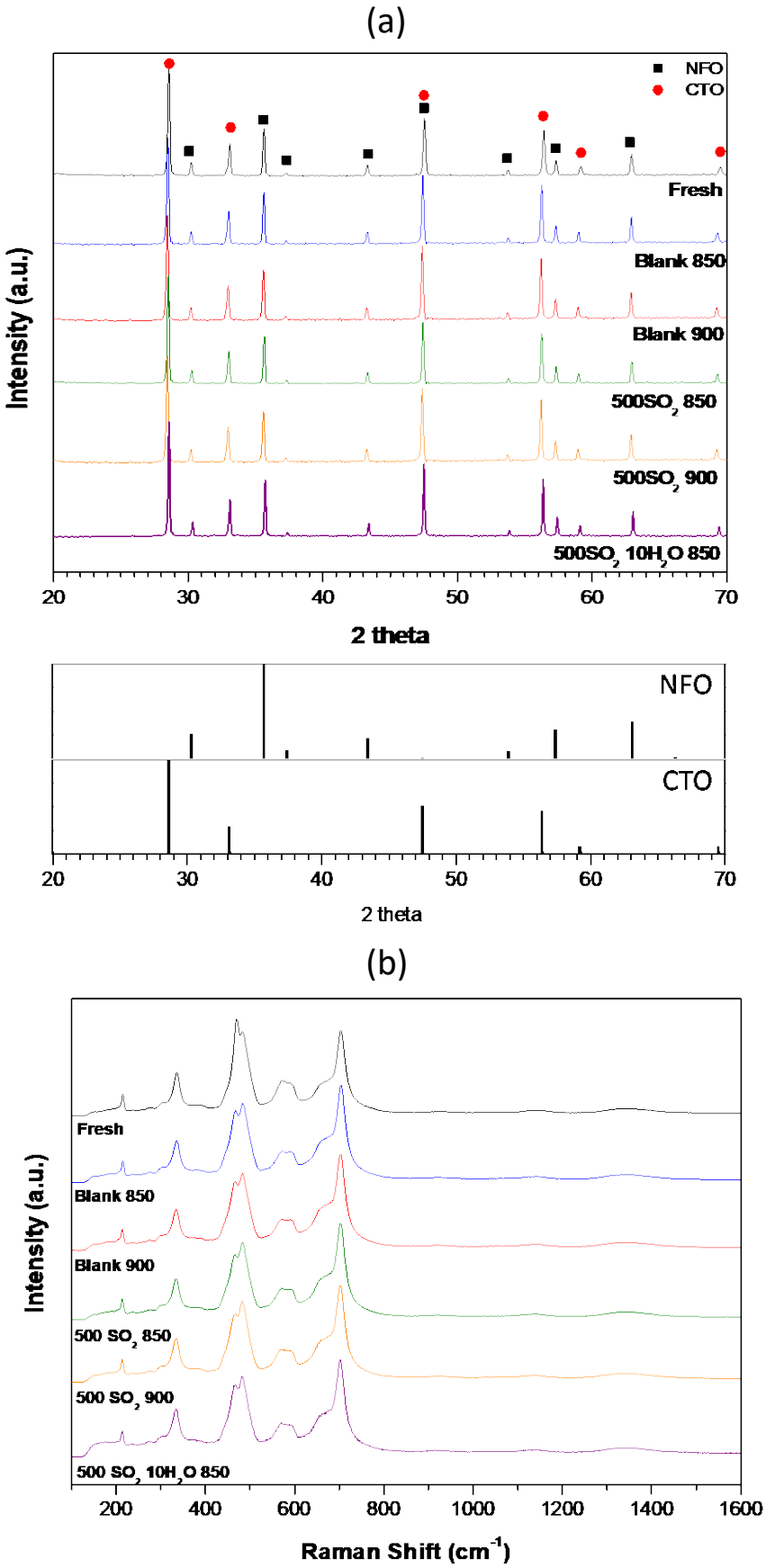

Figure 12. (a) XRD patterns; and (b) Raman spectra of the NFO-CTO powder samples fresh and treated with CO_2, CO_2/SO_2 and $CO_2/SO_2/H_2O$ mixtures at 850 and 900 ºC and atmospheric pressure

In the case of the NFO-CTO, no bands were observed in ATR-FTIR spectra of both fresh and spent samples (see Figure S4 in the supplementary material). For this reason, Raman is the only vibrational spectroscopy technique that has been used to study the possible formation of new species in the NFO-CTO after the exposure to CO_2, SO_2 and H_2O. Figure 12b shows the Raman spectra of the fresh and treated samples of NFO-CTO. The spectra of the treated samples were coincident with the fresh sample and only a slight change in the relative intensities of the peaks at 470 and 482 cm^{-1} could be observed. Ni and Fe sulphate peaks can be coincident with the peaks from the original NFO-CTO (in the range of 200-800 cm^{-1}), but these compounds also present several intense peaks in the range of 800-1400 cm^{-1} [42, 50, 54]. None of these signals were observed in the treated samples, and therefore the formation of these compounds was dismissed.

Figure 13 shows the XRD patterns and the Raman spectra of the NFO-CTO samples treated with different concentrations of SO_2 and H_2O at 850 ºC. In the same way as in the previous set of experiments, this material exhibited a completely different behaviour than that from LSCF. NFO-CTO did not show any modification after the treatment, regardless of the concentration of SO_2 and the H_2O content of the gas stream. Both the XRD (Figure 13a) and the Raman spectra (Figure 13b) of the treated samples were coincident with those from the fresh sample, which enabled discarding the formation of new species after the treatments. These results confirmed the high resistance of this composite against SO_2 and H_2O. NFO-CTO is able to work under concentrations of SO_2 and H_2O contents high enough to avoid the use of desulphurization and dewatering processes prior to the OTM module, which can avoid energy efficiency losses in the whole oxyfuel combustion process.

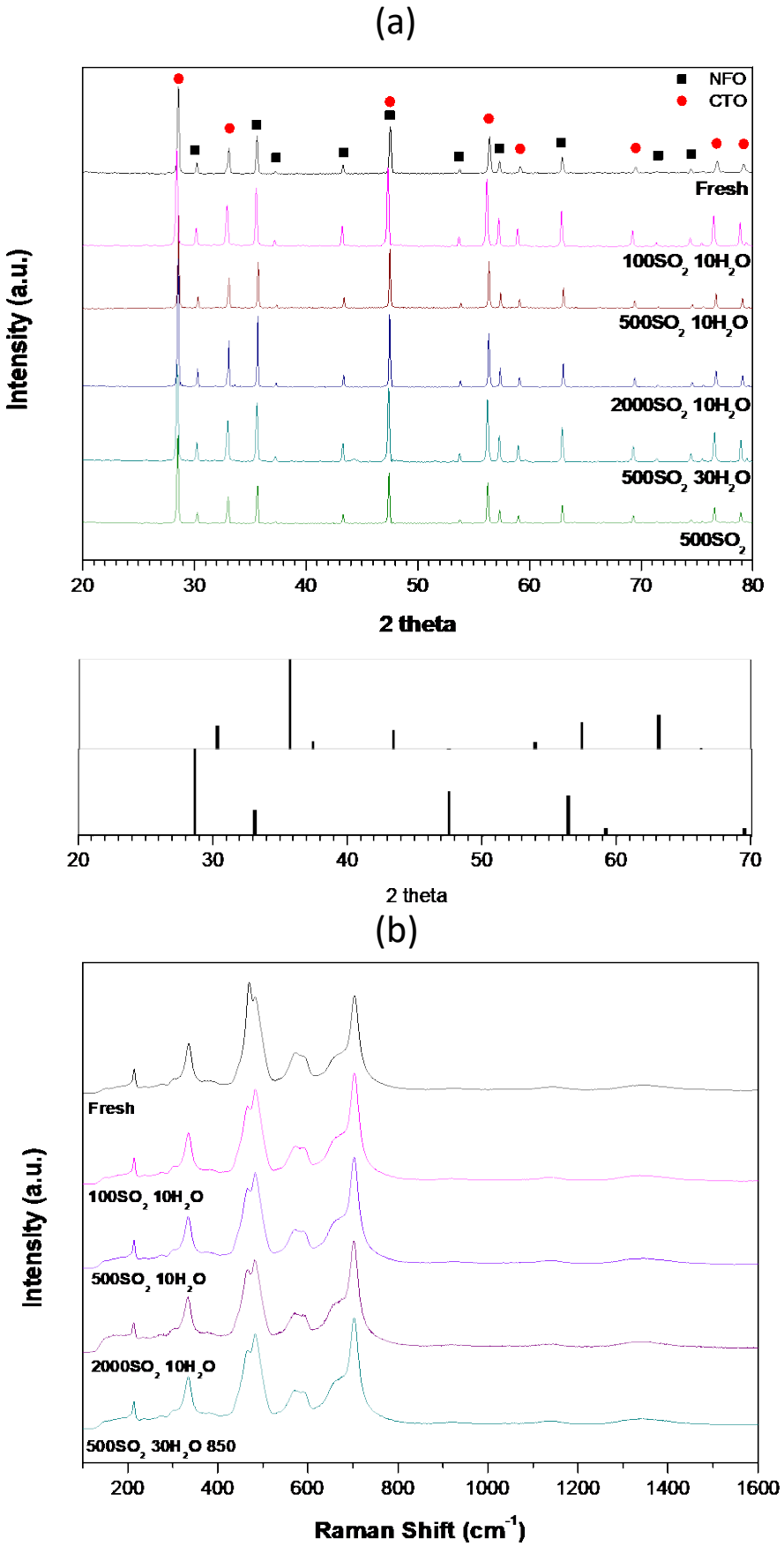

Figure 13. (a) XRD patterns; and (b) Raman spectra of the NFO-CTO powder samples fresh and treated under different concentrations of SO_2 and H_2O at 850 ºC and atmospheric pressure

Elemental analysis was used for discarding C and/or S incorporation to the treated NFO-CTO as any other species not identifiable by means of XRD or vibrational spectroscopy. Results are shown in Table 3. Contrary to the case of LSCF, none of these elements was found in the NFO-CTO samples, regardless of the treatment conditions. Therefore, incorporation of C or S in species not detectable by XRD or vibrational spectroscopies was also discarded. These results reinforced the conclusions that NFO-CTO is a composite resistant to the presence of CO_2, SO_2 and H_2O at high temperature.

3.2.2. Studies with dense sintered samples

The XRD of the as prepared NFO-CTO sample and the pattern after the stability test with 1000 ppm of SO_2 in N_2 are shown in Figure 14. The diffraction peaks were narrower and the contribution of Kα2 was observed more clearly in peaks at $2\theta > 45^{o}$, suggesting that the crystallinity of the material increased and pointing to some degree of coarsening in the two phases. Apart from this, there were no new peaks after the stability test. Consequently, the SO_2 exposure up to 1000 ppm and during 1000 h of testing did not lead to the formation of sulfates.

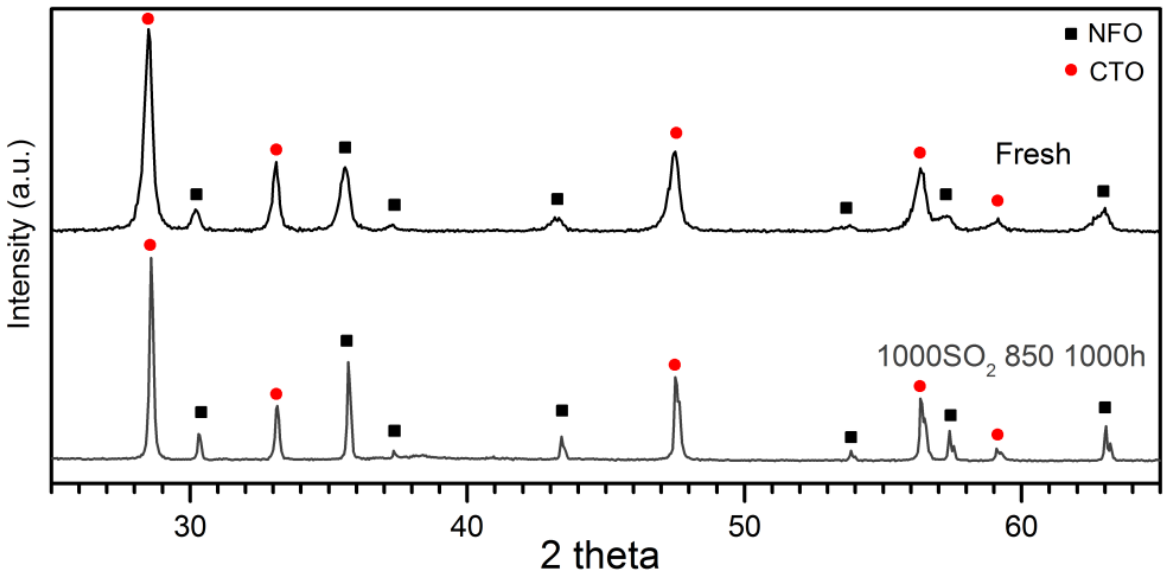

Figure 14. XRD patterns of the NFO-CTO sintered disks fresh and treated with 1000 ppm of SO_2 at 850 °C and atmospheric pressure

Although the resistance of NFO-CTO against the formation of new species has been demonstrated, it cannot be dismissed that sintering of the different phases (CTO or NFO) could occur during the treatment, e.g. changes in the grain morphology –coarsening–. In order to address this, the same

thermochemical stability tests performed with the powders were performed using small dense bars of the NFO-CTO composite. Those bars were analysed using SEM-EDS. SEM images of the cross-section of the original and the treated bars (in the harshest conditions: 2000 ppm SO_2/10 % H_2O and 500 ppm SO_2/30 % H_2O) are shown in Figure 15. In the high magnification backscattered pictures, it was possible to distinguish both NFO and CTO phases. In these images, the darker areas corresponded to the NFO (containing elements of lower atomic weight) whereas bright areas corresponded to the CGO (containing heavier elements). The distribution of both phases after the treatment remained homogeneous and no differences can be observed between the outer surfaces (marked with the white dashed box), which were directly exposed to the gaseous stream, and the inner surfaces, protected from the direct exposure to the gaseous stream. In addition, no significant differences between the original and the treated samples were observed. Only a slight increase in grain size was detected after the treatments. This slight increase in grain size was constant along the whole cross section of the bars. This suggested that no phase sintering occurred as a consequence of the interaction with the gases but as a consequence of the high temperature used in the treatment. The EDS spectra (available in Figure S5 from the Supporting Info) proved again that no sulphur was incorporated under any conditions.

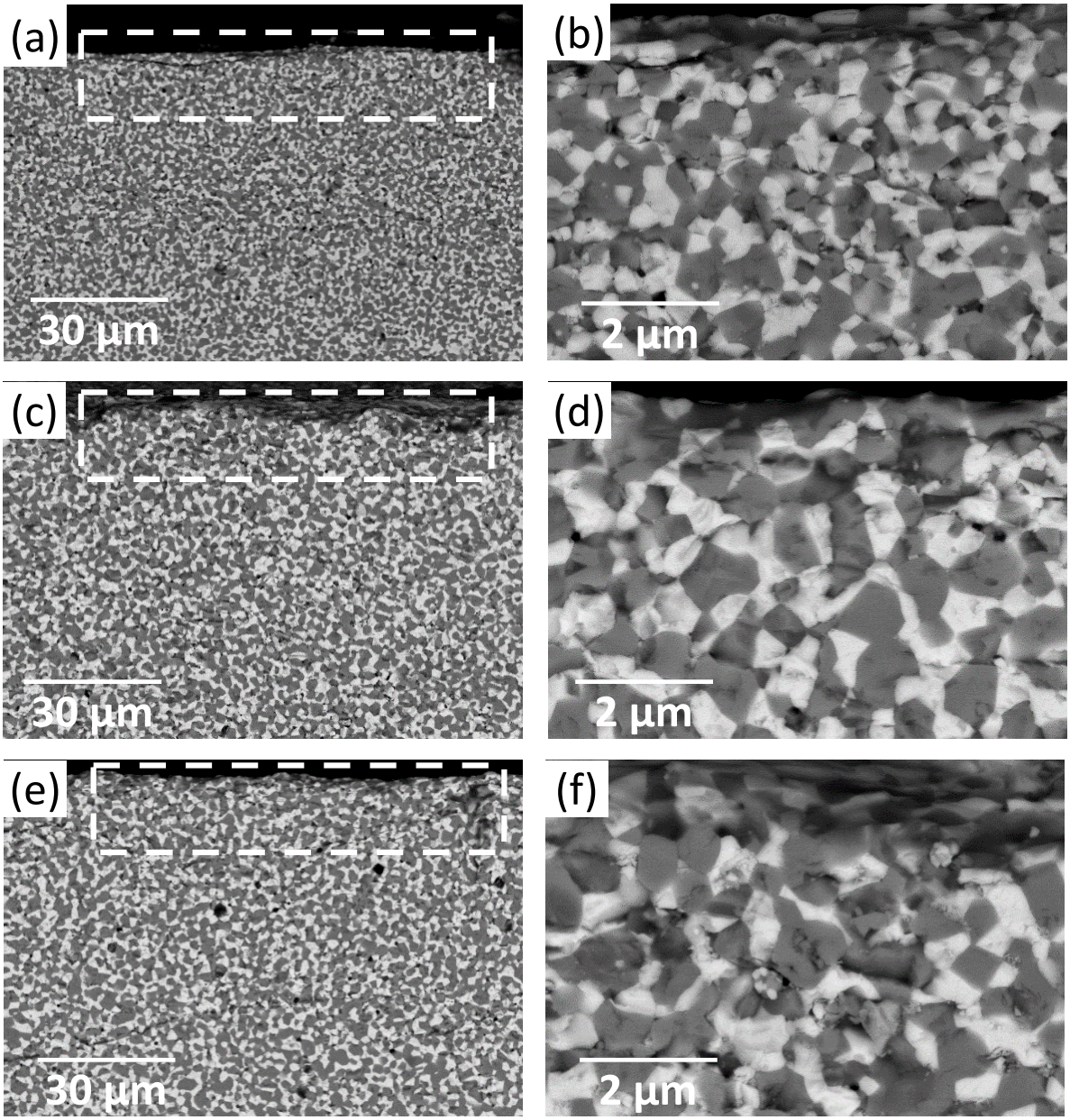

Figure 15. SEM images of cross sections from : original NFO-CTO bars at 1000X (a) and 5000X (b); NFO-CTO bars treated with 2000 ppm of SO_2 and 10% vol. of H_2O at 1000X (c) and 5000X (d); and NFO-CTO bars treated with 500 ppm of SO_2 and 30% vol. of H_2O at 1000X (e) and 5000X (f). The white dashed boxes indicate the outer surface that was in direct contact with the gaseous stream. EDS of the different areas analysed are provided in the Supplementary Information.

4. Conclusions

The dual-phase NFO-CTO composite has been found to be stable under operation conditions relevant to 4-end modules of OTMs. NFO-CTO has been tested under concentrations up to 2000 ppm of SO_2 in CO_2 and moisture contents up to 30 % vol. The composite does not undergo any modification,

regardless of the conditions studied, even in long-term experiments (time on stream up to 1000 h). On the contrary, single-phase LSCF perovskite has been tested under similar conditions showing poor thermochemical stability. When LSCF is put in contact with CO_2 and SO_2 it easily forms $SrCO_3$ and $SrSO_4$, respectively. The effect is especially severe in the case of SO_2 since a concentration of just 2000 ppm of SO_2 in CO_2 is able to almost completely prevent the formation of $SrCO_3$, segregating Sr from the perovskite structure only in the form of $SrSO_4$. Furthermore, the presence of SO_2 concentrations as low as 2 ppm is sufficient enough to form a $SrSO_4$ phase on the surface of LSCF.

With the results presented in this work, it is possible to conclude that the NFO-CTO composite is the preferred candidate (from the thermochemical stability point of view) to be used as mixed ionic-electronic conductor in 4-end modules of oxygen transport membranes for their application in oxyfuel combustion.

5. Acknowledgements

Financial support by the EU through FP7 GREEN-CC Project (Grant Agreement Number: 608524). The Spanish Government (ENE2014-57651 and SEV-2016-0683 grants) is gratefully acknowledged by JGF and JMS.

6. References

[1] M.B. Toftegaard, J. Brix, P.A. Jensen, P. Glarborg, A.D. Jensen, Oxy-fuel combustion of solid fuels, Progress in Energy and Combustion Science, 36 (2010) 581-625.
[2] T. Wall, Y. Liu, C. Spero, L. Elliott, S. Khare, R. Rathnam, F. Zeenathal, B. Moghtaderi, B. Buhre, C. Sheng, R. Gupta, T. Yamada, K. Makino, J. Yu, An overview on oxyfuel coal combustion-State of the art research and technology development, Chemical Engineering Research and Design, 87 (2009) 1003-1016.
[3] M.E. Boot-Handford, J.C. Abanades, E.J. Anthony, M.J. Blunt, S. Brandani, N. Mac Dowell, J.R. Fernández, M.C. Ferrari, R. Gross, J.P. Hallett, R.S. Haszeldine, P. Heptonstall, A. Lyngfelt, Z. Makuch, E. Mangano, R.T.J. Porter, M. Pourkashanian, G.T. Rochelle, N. Shah, J.G. Yao, P.S. Fennell, Carbon capture and storage update, Energy and Environmental Science, 7 (2014) 130-189.
[4] B.J.P. Buhre, L.K. Elliott, C.D. Sheng, R.P. Gupta, T.F. Wall, Oxy-fuel combustion technology for coal-fired power generation, Progress in Energy and Combustion Science, 31 (2005) 283-307.
[5] S. Smart, C.X.C. Lin, L. Ding, K. Thambimuthu, J.C. Diniz da Costa, Ceramic membranes for gas processing in coal gasification, Energy & Environmental Science, 3 (2010) 268-278.
[6] H.M. Kvamsdal, K. Jordal, O. Bolland, A quantitative comparison of gas turbine cycles with CO2 capture, Energy, 32 (2007) 10-24.
[7] R. Bredesen, K. Jordal, O. Bolland, High-temperature membranes in power generation with CO_2 capture, Chemical Engineering and Processing: Process Intensification, 43 (2004) 1129-1158.
[8] A. Leo, S. Liu, J.C.D.d. Costa, Development of mixed conducting membranes for clean coal energy delivery, International Journal of Greenhouse Gas Control, 3 (2009) 357-367.

[9] J. Sunarso, S. Baumann, J.M. Serra, W.A. Meulenberg, S. Liu, Y.S. Lin, J.C. Diniz da Costa, Mixed ionic-electronic conducting (MIEC) ceramic-based membranes for oxygen separation, Journal of Membrane Science, 320 (2008) 13-41.
[10] E. Turianicová, A. Obut, A. Zorkovská, P. Baláž, M. Matik, J. Briančin, The effects of LiOH and NaOH on the carbonation of SrSO4 by dry high-energy milling, Minerals Engineering, 49 (2013) 98-102.
[11] R. Kneer, D. Toporov, M. Förster, D. Christ, C. Broeckmann, E. Pfaff, M. Zwick, S. Engels, M. Modigell, OXYCOAL-AC: Towards an integrated coal-fired power plant process with ion transport membrane-based oxygen supply, Energy and Environmental Science, 3 (2010) 198-207.
[12] S. Engels, F. Beggel, M. Modigell, H. Stadler, Simulation of a membrane unit for oxyfuel power plants under consideration of realistic BSCF membrane properties, Journal of Membrane Science, 359 (2010) 93-101.
[13] J. Gao, L. Li, Z. Yin, J. Zhang, S. Lu, X. Tan, Poisoning effect of SO2 on the oxygen permeation behavior of La0.6Sr0.4Co0.2Fe0.8O3-δ perovskite hollow fiber membranes, Journal of Membrane Science, 455 (2014) 341-348.
[14] Y. Hu, J. Yan, Characterization of flue gas in oxy-coal combustion processes for CO2 capture, Applied Energy, 90 (2012) 113-121.
[15] J. Yi, S. Feng, Y. Zuo, W. Liu, C. Chen, Oxygen Permeability and Stability of Sr0.95Co0.8Fe0.2O3-δ in a CO2- and H2O-Containing Atmosphere, Chemistry of Materials, 17 (2005) 5856-5861.
[16] M. Arnold, H. Wang, A. Feldhoff, Influence of CO2 on the oxygen permeation performance and the microstructure of perovskite-type (Ba0.5Sr0.5)(Co0.8Fe0.2)O3−δ membranes, Journal of Membrane Science, 293 (2007) 44-52.
[17] E. Croiset, K.V. Thambimuthu, NOx and SO2 emissions from O2/CO2 recycle coal combustion, Fuel, 80 (2001) 2117-2121.
[18] J.C. Molburg, R.D. Doctor, N.F.S.P. Brockmeier, CO_2 capture from Pc boilers with O_2-firing, in: Eighteenth annual international Pittsburgh coal conference, Newcastle, Australia, 2001.
[19] J.-C. Chen, Z.-S. Liu, J.-S. Huang, Emission characteristics of coal combustion in different O2/N2, O2/CO2 and O2/RFG atmosphere, Journal of Hazardous Materials, 142 (2007) 266-271.
[20] H. Liu, Y. Shao, Predictions of the impurities in the CO2 stream of an oxy-coal combustion plant, Applied Energy, 87 (2010) 3162-3170.
[21] C. Spero, F. Montagner, L. Chapman, D. Ranie, T. Yamada, Callide Oxyfuel Project – Lessons Learned, in, Oxyfuel Technologies Pty Ltd, 2014.
[22] Y. Liu, T. Wall, S. Khare, R. Gupta, 9 - Oxy-fuel heat transfer characteristics and impacts on boiler design A2 - Zheng, Ligang, in: Oxy-Fuel Combustion for Power Generation and Carbon Dioxide (Co2) Capture, Woodhead Publishing, 2011, pp. 166-194.
[23] S. Baumann, J.M. Serra, M.P. Lobera, S. Escolástico, F. Schulze-Küppers, W.A. Meulenberg, Ultrahigh oxygen permeation flux through supported Ba0.5Sr0.5Co0.8Fe0.2O3−δ membranes, Journal of membrane Science, 377 (2011) 198-205.
[24] J.M. Serra, J. Garcia-Fayos, S. Baumann, F. Schulze-Kueppers, W.A. Meulenberg, Oxygen permeation through tape-cast asymmetric all-La0.6Sr0.4Co0.2Fe0.8O3 (-) (delta) membranes, Journal of Membrane Science, 447 (2013) 297-305.
[25] J. Yi, M. Schroeder, High temperature degradation of Ba0.5Sr0.5Co0.8Fe0.2O3-delta membranes in atmospheres containing concentrated carbon dioxide, Journal of Membrane Science, 378 (2011) 163-170.
[26] S. Engels, T. Markus, M. Modigell, L. Singheiser, Oxygen permeation and stability investigations on MIEC membrane materials under operating conditions for power plant processes, Journal of Membrane Science, 370 (2011) 58-69.
[27] J. Gao, L. Li, Z. Yin, J. Zhang, S. Lu, X. Tan, Poisoning effect of SO2 on the oxygen permeation behavior of La0.6Sr0.4Co0.2Fe0.8O3−δ perovskite hollow fiber membranes, Journal of Membrane Science, 455 (2014) 341-348.

[28] R.R. Liu, S. Taniguchi, Y. Shiratori, K. Ito, K. Sasaki, Influence of SO2 on the Long-term Durability of SOFC Cathodes, in: S.C. Singhal, K. Eguchi (Eds.) Solid Oxide Fuel Cells 12, 2011, pp. 2255-2260.
[29] F. Wang, K. Yamaji, D.H. Cho, T. Shimonosono, M. Nishi, H. Kishimoto, M.E. Brito, T. Horita, H. Yokokawa, Evaluation of Sulfur Dioxide Poisoning for LSCF Cathodes, Fuel Cells, 13 (2013) 520-525.
[30] F.F. Wang, H. Kishimoto, K. Develos-Bagarinao, K. Yamaji, T. Horita, H. Yokokawa, Interrelation between Sulfur Poisoning and Performance Degradation of LSCF Cathode for SOFCs, Journal of the Electrochemical Society, 163 (2016) F899-F904.
[31] E. Bucher, C. Gspan, W. Sitte, Degradation and regeneration of the SOFC cathode material La0.6Sr0.4CoO3-delta in SO2-containing atmospheres, Solid State Ionics, 272 (2015) 112-120.
[32] E. Bucher, C. Gspan, F. Hofer, W. Sitte, Sulphur poisoning of the SOFC cathode material La0.6Sr0.4CoO3-delta, Solid State Ionics, 238 (2013) 15-23.
[33] S.J. Benson, D. Waller, J.A. Kilner, Degradation of La0.6Sr0.4Fe0.8Co0.2 O 3 − δ in Carbon Dioxide and Water Atmospheres, Journal of The Electrochemical Society, 146 (1999) 1305-1309.
[34] R. Wang, B. Meng, X. Meng, X. Tan, J. Sunarso, L. Liu, S. Liu, Highly stable La0.6Sr0.4Co0.2Fe0.8O3-δ hollow fibre membrane for air separation swept by steam or steam mixture, Journal of Membrane Science, 479 (2015) 232-239.
[35] Z. Zhao, L. Liu, X. Zhang, W. Wu, B. Tu, D. Cui, D. Ou, M. Cheng, High- and low- temperature behaviors of La0.6Sr0.4Co0.2Fe0.8O3−δ cathode operating under CO2/H2O-containing atmosphere, International Journal of Hydrogen Energy, 38 (2013) 15361-15370.
[36] E. Bucher, W. Sitte, Long-term stability of the oxygen exchange properties of (La,Sr)1 − z(Co,Fe)O3 − δ in dry and wet atmospheres, Solid State Ionics, 192 (2011) 480-482.
[37] K. Efimov, T. Klande, N. Juditzki, A. Feldhoff, Ca-containing CO2-tolerant perovskite materials for oxygen separation, Journal of Membrane Science, 389 (2012) 205-215.
[38] Q. Jiang, S. Faraji, D.A. Slade, S.M. Stagg-Williams, Chapter 11 - A Review of Mixed Ionic and Electronic Conducting Ceramic Membranes as Oxygen Sources for High-Temperature Reactors, in: S.T. Oyama, M.S.-W. Susan (Eds.) Membrane Science and Technology, Elsevier, 2011, pp. 235-273.
[39] W. Fang, F. Liang, Z. Cao, F. Steinbach, A. Feldhoff, A Mixed Ionic and Electronic Conducting Dual-Phase Membrane with High Oxygen Permeability, Angewandte Chemie International Edition, 54 (2015) 4847-4850.
[40] J. Garcia-Fayos, M. Balaguer, J.M. Serra, Dual-Phase Oxygen Transport Membranes for Stable Operation in Environments Containing Carbon Dioxide and Sulfur Dioxide, ChemSusChem, (2015).
[41] H. Luo, K. Efimov, H. Jiang, A. Feldhoff, H. Wang, J. Caro, CO2-Stable and Cobalt-Free Dual-Phase Membrane for Oxygen Separation, Angewandte Chemie International Edition, 50 (2011) 759-763.
[42] M. Balaguer, J. García-Fayos, C. Solís, J.M. Serra, Fast Oxygen Separation Through SO2- and CO2-Stable Dual-Phase Membrane Based on NiFe2O4–Ce0.8Tb0.2O2-δ, Chemistry of Materials, 25 (2013) 4986-4993.
[43] C. Gaudillere, J. Garcia-Fayos, M. Balaguer, J.M. Serra, Enhanced Oxygen Separation through Robust Freeze-Cast Bilayered Dual-Phase Membranes, Chemsuschem, 7 (2014) 2554-2561.
[44] M. Balaguer, J. Garcia-Fayos, C. Solis, J.M. Serra, Fast oxygen separation through SO2- and CO2-stable dual-phase membranes based on NiFe2O4-Ce0.8Tb0.2O2-δ, Chemistry of Materials, (2013).
[45] J. Garcia-Fayos, M. Balaguer, J.M. Serra, Dual-Phase Oxygen Transport Membranes for Stable Operation in Environments Containing Carbon Dioxide and Sulfur Dioxide, ChemSusChem, (2015) n/a-n/a.
[46] J.M. Serra, V.B. Vert, M. Betz, V.A.C. Haanappel, W.A. Meulenberg, F. Tietz, Screening of A-substitution in the system A(0.68)Sr(0.3)Fe(0.8)Co(0.2)O(3-delta) for SOFC cathodes, Journal of the Electrochemical Society, 155 (2008) B207-B214.
[47] Y. Yu, H. Luo, D. Cetin, X. Lin, K. Ludwig, U. Pal, S. Gopalan, S. Basu, Effect of atmospheric CO2 on surface segregation and phase formation in La0.6Sr0.4Co0.2Fe0.8O3−δ thin films, Applied Surface Science, 323 (2014) 71-77.

[48] X. Tan, N. Liu, B. Meng, J. Sunarso, K. Zhang, S. Liu, Oxygen permeation behavior of La0.6Sr0.4Co0.8Fe0.2O3 hollow fibre membranes with highly concentrated CO2 exposure, Journal of Membrane Science, 389 (2012) 216-222.
[49] C.C. Wang, K. Chen, S.P. Jiang, Sulfur deposition and poisoning of la0.6Sr0.4Co0.2Fe0.8O3-δ cathode materials of solid oxide fuel cells, Journal of the Electrochemical Society, 161 (2014) F1133-F1139.
[50] K. Nakamoto, Infrared and Raman spectra of inorganic and coordination compounds, Wiley Online Library, 1986.
[51] M.E. Böttcher, P.-L. Gehlken, Á. Fernández-González, M. Prieto, Characterization of synthetic BaCO3–SrCO3 (witherite-strontianite) solid-solutions by Fourier transform infrared spectroscopy, European Journal of Mineralogy, (1997) 519-528.
[52] B. Hu, M.K. Mahapatra, M. Keane, H. Zhang, P. Singh, Effect of CO2 on the stability of strontium doped lanthanum manganite cathode, Journal of Power Sources, 268 (2014) 404-413.
[53] A. Periasamy, S. Muruganand, M. Palaniswamy, Vibrational studies of Na2SO4, K2SO4, NaHSO4 and KHSO4 crystals, Rasayan Journal of Chemistry, 2 (2009) 981-989.
[54] R. Cui, D. Li, X. Fu, M. Asif, L. Pan, Growth of a Carbon Micro- and Nanocoils Mixture using NiSO4 as the Catalyst Precursor, Chemical Vapor Deposition, 21 (2015) 78-83.
[55] T. Ramirez-Reina, J.L. Santos, N. García-Moncada, S. Ivanova, J.A. Odriozola, Development of Robust Mixed-Conducting Membranes with High Permeability and Stability, in: Perovskites and Related Mixed Oxides, Wiley-VCH Verlag GmbH & Co. KGaA, 2016, pp. 719-738.
[56] C. Chatzichristodoulou, M. Søgaard, J. Glasscock, A. Kaiser, S.P.V. Foghmoes, P.V. Hendriksen, Oxygen Permeation in Thin, Dense Ce0.9Gd0.1O1.95-δ Membranes II. Experimental Determination, Journal of The Electrochemical Society, 158 (2011) F73-F83.
[57] H. Luo, K. Efimov, H. Jiang, A. Feldhoff, H. Wang, J. Caro, CO2-stable and cobalt-free dual-phase membrane for oxygen separation, Angewandte Chemie - International Edition, 50 (2011) 759-763.
[58] B. Wang, G. Xiao, X. Song, H. Zhao, C. Zheng, Chemical looping combustion of high-sulfur coal with NiFe2O4-combined oxygen carrier, Journal of Thermal Analysis and Calorimetry, 118 (2014) 1593-1602.
[59] M. Waqif, P. Bazin, O. Saur, J.C. Lavalley, G. Blanchard, O. Touret, Study of ceria sulfation, Applied Catalysis B: Environmental, 11 (1997) 193-205.
[60] M. Waqif, A.M. Saad, M. Bensitel, J. Bachelier, O. Saur, J.-C. Lavalley, Comparative study of SO2 adsorption on metal oxides, Journal of the Chemical Society, Faraday Transactions, 88 (1992) 2931-2936.
[61] T. Luo, R.J. Gorte, Characterization of SO2-poisoned ceria-zirconia mixed oxides, Applied Catalysis B: Environmental, 53 (2004) 77-85.
[62] Q. Xue, L. Gao, Y. Lu, Sulfur-tolerant Pt/Gd2O3–CeO2–Al2O3 catalyst for high efficiency H2 production from autothermal reforming of retail gasoline, Catalysis Today, 146 (2009) 103-109.
[63] J.A. Rodriguez, T. Jirsak, A. Freitag, J.C. Hanson, J.Z. Larese, S. Chaturvedi, Interaction of SO2 with CeO2 and Cu/CeO2 catalysts: photoemission, XANES and TPD studies, Catalysis Letters, 62 (1999) 113-119.
[64] J.H. Kwak, D.H. Kim, J. Szanyi, C.H.F. Peden, Excellent sulfur resistance of Pt/BaO/CeO2 lean NOx trap catalysts, Applied Catalysis B: Environmental, 84 (2008) 545-551.
[65] P. Boldrin, E. Ruiz-Trejo, J. Mermelstein, J.M. Bermúdez Menéndez, T. Ramírez Reina, N.P. Brandon, Strategies for Carbon and Sulfur Tolerant Solid Oxide Fuel Cell Materials, Incorporating Lessons from Heterogeneous Catalysis, Chemical Reviews, 116 (2016) 13633-13684.
[66] A.M. Banerjee, M.R. Pai, S.S. Meena, A.K. Tripathi, S.R. Bharadwaj, Catalytic activities of cobalt, nickel and copper ferrospinels for sulfuric acid decomposition: The high temperature step in the sulfur based thermochemical water splitting cycles, International Journal of Hydrogen Energy, 36 (2011) 4768-4780.

For Table of Contents Only

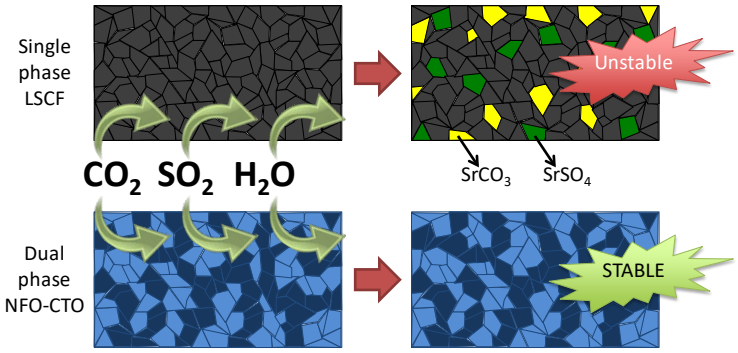

Synopsis

The thermochemical stability of two mixed ionic-electronic conductors has been tested under real operating conditions in 4-end modules of oxygen transport membranes for application in oxyfuel combustion. It has been found that the dual-phase NFO-CTO is stable under all the conditions tested whereas the single phase LSCF shows low stability, reacting with CO_2 and SO_2 to form carbonates and sulphates.